

Pseudo-capacitive Behavior of Graphene Oxide Paper in AlCl_3 and 1-ethyl-3-methylimidazolium Chloride (Molar Ratio of 1.3:1) Solution and its Application for Aluminium Ion Batteries

Jia Qiao^{1,*}, Juan Du¹, Zhongsheng Liu², Haitao Zhou², Hejing Wen², Chao Liu², Jianhong Yang^{1,2,*}

¹ School of Metallurgy and Environment, Central South University, Changsha 410000, PR China

² School of Materials Science and Engineering, Jiangsu University, Zhenjiang 212000, PR China

*E-mail: john_39842@163.com (Jia Qiao); jhyang_qx@yahoo.com (Jianhong Yang)

Received: 7 June 2019 / Accepted: 18 July 2019 / Published: 30 August 2019

Graphene-based materials are cathodes of Al-ion batteries and have attracted the attention of researchers worldwide. However, reasons for self-discharge in Al/graphene batteries have not been studied in depth. In the present work, a pseudo-capacitive reaction is proposed to be a probable cause of the self-discharge. Quantitative analysis of the capacitance process and diffusion-control process is critical for the pseudo-capacitive behavior in Al/graphene batteries. Two self-supported graphene cathodes (R_H-GOP and R_N-GOP) were successfully produced from graphene oxides (GO) reduced with hydriodic acid and hydrazine vapor, respectively. R_H-GOP and R_N-GOP cathodes enabled the delivery of considerably high specific capacities of 81.5 mAh g⁻¹ and 92.8 mAh g⁻¹, at the current density of 2 A g⁻¹. In addition, the activation processes of both materials were observed during 200 cycles of the charge-discharge process. From a quantitative perspective, the ratios of faradaic pseudo-capacitance to the total capacity of the R_H-GOP and R_N-GOP cathode were 48.6% and 38.5%, respectively, at a scanning rate of 5.0 mV s⁻¹. It is found that the proportion of faradaic pseudo-capacitance will increase as cyclic voltammetry scanning increases, which indicates the existence of pseudo-capacitance being the reason why it an Al/graphene battery has to be charged-discharged at high current densities to maintain normal operation.

Keywords: Al-ion battery; Oxide graphene paper; Cathode; Pseudocapacitive; self-discharge

1. INTRODUCTION

Aluminium, the most abundant metal in Earth's crust (8.13%), is exploited more than 1,000 times more than lithium worldwide. It would greatly reduce the production cost of batteries if Al was used as an electrode material for secondary batteries instead of Li [1,2]. In the past 30 years, research on aluminium ion batteries (AIBs) has been ongoing, but few achievements have been made. Since it was reported in 2005, AIBs have attracted interest worldwide [3]. In 2011, Archer's research group

reported that a specific capacity of 270 mAh g⁻¹ for AIBs was achieved with [EMIm]/AlCl₃ ionic liquid (ILs) as the electrolyte and V₂O₅ as the cathode material [4]. However, the accuracy of the positive electrode reaction is still questionable. The application of [EMIm]/AlCl₃ ILs in AIBs promoted the progress of AIBs. Based on previous research, Dai first reported a stable Al/graphene battery with [EMIm]/AlCl₃ ILs as the electrolyte and CVD three-dimensional flexible graphene as the cathode, representing a new breakthrough in the field of AIBs. The battery exhibited a high power density of 3000 W kg⁻¹, which was comparable with that of a supercapacitor [5]. Although the battery reported by Dai was only a prototype, it has blown a horn for the research of AIBs. Currently, AIBs have gradually become the focus of large-scale energy storage research because of the application of ILs as electrolytes.

Graphite and carbon-containing materials are expected to be cathode materials with special van der Waals force connections between graphite layers in which the AlCl₄⁻ ion can be stably inserted into the graphitized structure [6,7]. From this perspective, graphite [8-13], carbon-graphite [14,15], polypyrenes [16], 3D foamed graphite [17], mesoporous carbon materials and graphene [7,18-24] have been tested as cathode materials of AIBs. In particular, over the past four years, the research activity of AIBs graphene cathodes has surged, which has undeniably led to significant progress in this field [5,20]. Graphene cathode materials have many advantages compared with other cathodes. First, the discharge potential of the graphene cathode to Al/Al³⁺ exceeds 1.8 V, which is higher than other transition metal oxide/sulfide cathodes (< 1 V vs. Al/Al³⁺) [22,25]. Second, the graphene cathode has ultra-high rate performance (400 A g⁻¹, 120 mAh g⁻¹) [21]. The high-power density is very suitable for power battery applications such as automotive start-stop and power grid storage. Third, the stability of the graphene cathode is very prominent. The Al/graphene battery can be stabilized for more than 250,000 cycles with little change in energy and power density [21]. Although carbon materials have relatively low capacities compared with sulfide and oxide cathode materials, their high stability and rate performance make them more likely to be commercialized in AIBs. Yu [19] suggested a method to significantly enhance the AlCl₄⁻ ion storage capacity of 3D graphene foam by Ar⁺-plasma etching. This resulted in a higher discharge capacity of 123 mAh g⁻¹ at a current rate of 5 A g⁻¹ (Coulombic efficiency > 98%). Gao [20] annealed graphene at 3000°C to obtain a defect-free graphene cathode material. The as-prepared Al/graphene had a specific capacity of 100 mAh g⁻¹ and could maintain 97% capacity after 25,000 cycles of charge-discharge. Wang [12] reported high-quality natural flake graphite as a cathode material after CVD pretreatment of three-dimensional flexible graphite (660 mA g⁻¹, 110 mAh g⁻¹). The Al/graphite battery had a capacity retention rate of over 99% after 6,000 cycles, which confirmed that defect-free graphitic materials have better performance as cathodes of AIBs.

Although the highly reversible and stable Al/graphene battery has been confirmed, all of the reports [5,19-21,26] do not have charge-discharge tests at low current density, and previous reports [6,7,10] considered Al/graphene batteries behaving as a pseudo-capacitor, which explains why self-discharge occurs in Al/graphene batteries. Therefore, it is necessary to carry out more meticulous research on the existence of capacitance control processes and diffusion-control processes in AIBs. In this paper, self-supporting graphene oxide paper (GOP) was prepared using graphene oxide (GO) as a raw material by vacuum filtration. The GOP was chemically reduced with two relatively common chemical reduction methods (HI and N₂H₄) to obtain two cathode materials (R_H-GOP and R_N-GOP)

(Fig. 1). The quantitative analysis of the capacitance control process and the diffusion-control process of AIBs was carried out, which could be a reference to subsequent research.

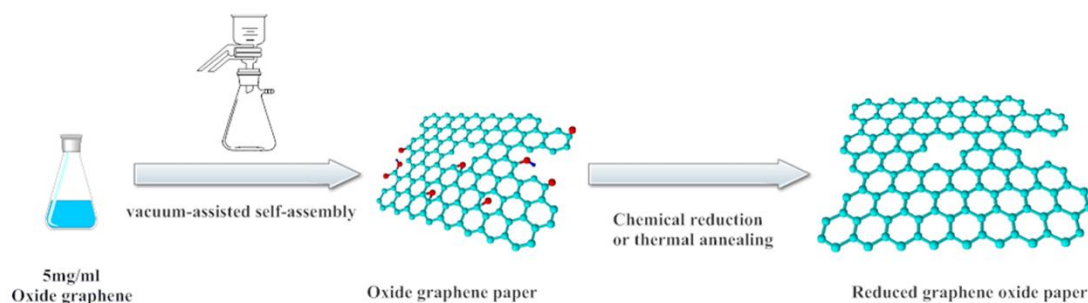


Figure 1. Schematic diagram of the preparation process of the cathode material.

2. EXPERIMENTAL DETAILS

2.1 Preparation of GO and GOP

GO was obtained to use the modified Hummers method. Raw materials include natural graphite powder (SP-1, Bay Carbon, MI), H_2SO_4 (95.0~98.0%, Sinopharm), NaNO_3 (>99.0%, Sinopharm), KMnO_4 (>99.5%, Sinopharm), HCl (36.0~38.0%, Sinopharm) and H_2O_2 ($\geq 30.0\%$, Sinopharm). The final prepared GO concentration was 5 mg ml^{-1} . GOP was obtained by vacuum filtration [27,28], and an Anodisc film (25 mm in diameter, $0.2 \mu\text{m}$ pore size, Whatman) was used as a membrane. The thickness could be controlled by adjusting the weight of the GO additive, and the filtered membrane was air dried and then peeled off.

2.2 Electrode preparation

GOP was immersed in Hydroiodic acid (55.0 ~ 58.0%, Aladdin) at 100°C for 1 hour to obtain a R_H -GOP electrode [29]. The R_N -GOP electrode was obtained by using GOP at $\text{N}_2\text{H}_4 \cdot \text{H}_2\text{O}$ (80.0%, Aladdin) vapor at 90°C for 24 hours [28].

2.3 Characterization

The crystal phases of the resulting materials were analyzed by X-ray diffraction (XRD, Rigaku, D/max-2500/PC). Raman spectroscopy was recorded on a Renishaw Raman spectrometer using an Ar laser with a wavelength of 514 nm. XPS (X-ray photoelectron spectroscopy) analysis was conducted on a SIGMA PROBE (ThermoVG) instrument using monochromatic $\text{Al-K}\alpha$ X-ray radiation. The morphologies of the samples were investigated by SEM (scanning electron microscopy, JEOL JEM-7800F).

2.4 Electrochemical measurement

The thin R_H-GOP and R_N-GOP composite slices could be used as a binder-free electrode for AIBs that do not require any binding material. The pouch cells were assembled in an argon-filled glovebox (H₂O and O₂ < 0.1 ppm) to avoid any contact with moisture or air. The electrolyte used AlCl₃ (Sigma-Aldrich, 99.999%) and 1-ethyl-3-methylimidazolium chloride ([EMIm]Cl, Aladdin, 98%) mixed at a molar ratio of 1.3:1. The pouch cells were galvanostatic charged-discharged between 0.5 and 2.4 V (*vs.* Al/Al⁺³) by using a cell test instrument (NEWARE, Shenzhen). The cyclic voltammetry (CV) measurements were taken with a PARSTAT MC (Princeton Applied Research).

3. RESULTS AND DISCUSSION

Fig. 2 shows SEM images and cross-views of GOP (Figs. 2a, b), R_H-GOP (Figs. 2c, d) and R_N-GOP (Figs. 2e, f). It can be seen from Fig. 2a that there is a wrinkle-like surface on the GOP before reduction. There is no obvious change in the morphology of R_H-GOP (Fig. 2c) after being reduced by HI from GOP. After hydrazine vapor reduction, a rougher surface and many apparent cracks are observed on the surface of R_N-GOP (Fig. 2e). Compared with the GOP (Fig. 2b), the R_H-GOP thickness (Fig. 2d) does not change significantly, while the R_N-GOP (Fig. 2f) typically expanded tens of times after the hydrazine vapor. The reason for the above changes is mainly because a large number of functional groups of GOP become damaged by gas, leaving a paper material [28].

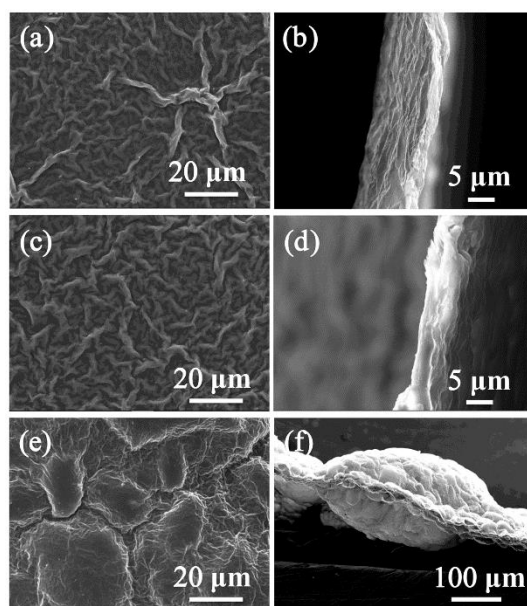


Figure 2. SEM images and cross-section views of various paper samples. (a, b) Original GOP, (c, d) R_H-GOP, (e, f) R_N-GOP.

The X-ray diffraction patterns of the GOP, R_H-GOP and R_N-GOP samples are shown in Fig. 3a. The XRD spectrum reveals that only one peak at $2\theta = 11.3^\circ$ can be detected, which is due to the

oxidation effect adhering to the surface of the GOP sheet. After HI reduction, the 2θ peaks of R_H -GOP are 13.9° and 24.7° , which correspond to interlayer distances of 0.639 nm and 0.361 nm, respectively. Similarly, after hydrazine vapor reduction, the 2θ peaks of R_N -GOP are 14.4° (0.612 nm) and 26.43° (0.336 nm). The reason for these reductions is attributed to overflowing the oxygen-containing functional groups and water molecules. This reduction result is also confirmed by Raman spectra and XPS patterns. In general, Raman spectra are used to observe the defects of graphene oxide paper, which plays a significant role in the characterization of graphitization. Both the D-band and G-band in the Raman spectra (Fig. 3b) are observed in all three samples, and the D-band in the reduced samples is significantly increased. The D-band ($\sim 1360\text{ cm}^{-1}$) in all samples of the Raman spectra confirmed defects and disorder, while the G-band ($\sim 1580\text{ cm}^{-1}$) is the characteristic of sp^2 hybridized carbon-carbon bonds in graphene. The I_D/I_G ratio of R_H -GOP and R_N -GOP exhibited a significant increase compared to GOP, which is consistent with other studies [30]. In addition, Rao [31] thought that the I_D/I_G ratio does not always reflect the oxidation or reduction degree, because the I_D/I_G ratio can be ripples, charge puddles, influence by edges, or many other defects. Due to the limitations of Raman spectroscopy in the study of GOP, XPS spectroscopy becomes a necessary analysis.

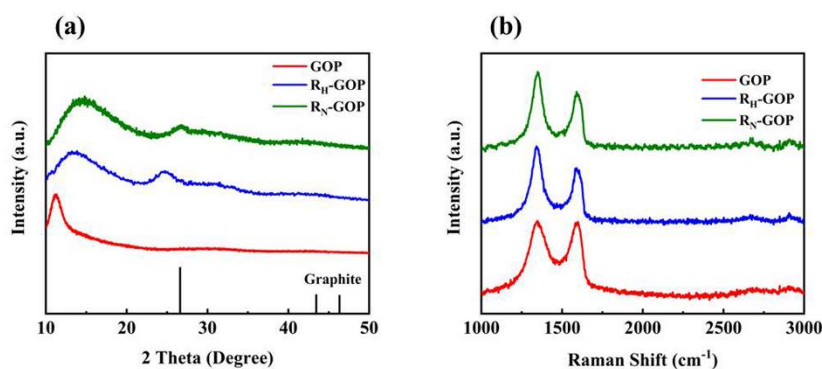


Figure 3. (a) XRD patterns and (b) Raman spectra of GOP, R_H -GOP and R_N -GOP.

XPS is an effective surface chemical analysis technique, that is used to determine the elemental content and functional group of the three samples. Fig. 4a is a full spectrum XPS scan of all the samples above, which indicates a summary of the percentages of C, O, N and I atoms and the C/O ratio surface compositions (seen in Table 1). The C1s spectrum of GOP (Fig. 4b) reveals that there are two main components at 284.6 eV and 286.5 eV arising from C-C (sp^3) and C-O (including epoxide (-O-) and hydroxyl (-OH)), and two minor components corresponding to C=O (carbonyl, ~ 288.3 eV) and O-C=O (carboxyl, ~ 290.3 eV) groups [29]. The C1s XPS spectra of R_H -GOP and R_N -GOP (as shown in Figs. 4c, d) exhibit the same oxygen-containing functional groups that have been assigned for GOP, while some peak intensities of these components in R_H -GOP and R_N -GOP samples are much smaller than those in the GOP, indicating considerable deoxygenation by the reduction process. Luo [28] reported that the primary role of a reducing agent (eg. N_2H_4) is turning C=O into C-O, and the ratio of the C-O/C-C has increased after chemical reduction. Specifically, most of the C-C (sp^3) bonds at 284.6 eV are converted to C-C (sp^2) (284.0 eV) by chemical reduction. However, it can be clearly observed

that the C-C (sp^3) in R_H-GOP is significantly reduced, indicating that HI is a more effective means of reduction. In addition, the changes in the C/O ratio of R_H-GOP and R_N-GOP samples indicate different reduction degrees (Table 1).

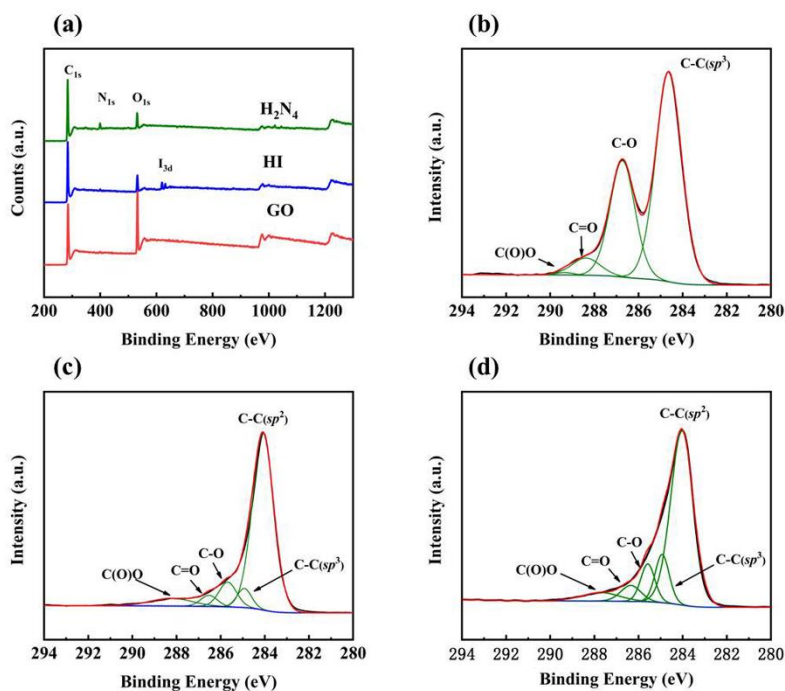


Figure 4. (a) XPS spectra of GOP, R_H-GOP and R_N-GOP. C1s spectra of (b) GOP, (c) R_H-GOP, (d) R_N-GOP.

Table 1. XPS analysis of C, O, N, I content and calculated C/O ratios for GO-P, R_H-GOP and R_N-GOP paper samples.

| Sample | C (at.%) | O (at.%) | N (at.%) | I (at.%) | C/O |
|--------------------|----------|----------|----------|----------|------|
| GOP | 72.86 | 27.14 | - | - | 2.68 |
| R _H G-P | 88.82 | 10.88 | - | 0.30 | 8.16 |
| R _N G-P | 82.99 | 11.30 | 5.71 | - | 7.34 |

The electrochemical performances of the Al/R_H-GOP and Al/R_N-GOP batteries are investigated in pouch cell configurations. Figs. 5 (a, b) shows the charge-discharge curves of R_H-GOP and R_N-GOP as cathode materials for AIBs at a current density of 2 A g⁻¹. The charge-discharge curves show that the AIBs prepared by the two samples have many similarities. First of all, the charge-discharge curves of Al/R_H-GOP and Al/R_N-GOP batteries have no obvious voltage platform, which is similar to the previously reported battery [23]. In addition, the batteries have a low initial discharge specific capacity of 5.8 mAh g⁻¹ (R_H-GOP) and 3.7 mAh g⁻¹ (R_N-GOP). Therefore, both cathode materials require a charge/discharge activation process to maximize the specific capacity of the battery. It is difficult to explain this result, but it might be related to poor wetting of graphite and [EMIm]/AlCl₃ ILs. In fact, a strong relationship between discharge capacity and electrode thickness has been reported in the

literature [12]. There are, however, other possible explanations. In general, the precursor for the preparation of both cathode materials is GO, and the GOP is chemically reduced without graphite crystallization. Therefore, the charge-discharge curves of Al/R_H-GOP (or Al/R_N-GOP) batteries are different from those of other Al/graphene batteries [12,15]. Interestingly, the highest discharge specific capacity of the Al/R_N-GOP battery is the 63rd cycle (92.8 mAh g⁻¹), while the highest discharge capacity of the Al/R_H-GOP battery is the 16th cycle (81.5 mAh g⁻¹). This indicated that the R_N-GOP requires more charge-discharge to release the specific capacity of the battery and achieve a higher specific capacity in the following charge-discharge process. The phenomenon above may be attributed to the fact that the hydrazine vapor chemical reduction is beneficial for increasing the specific surface area of R_N-GOP (Figs. 2e, f). The larger specific surface area of the cathode material indicates more active sites, which contribute to sufficient wetting of the ILs electrolyte and higher specific capacity. At the same time, R_N-GOP a more closed pore structure, and the electrolyte cannot quickly wet all electrochemically active sites. Therefore, it takes a long activation time to achieve the full specific capacity of R_N-GOP AIB.

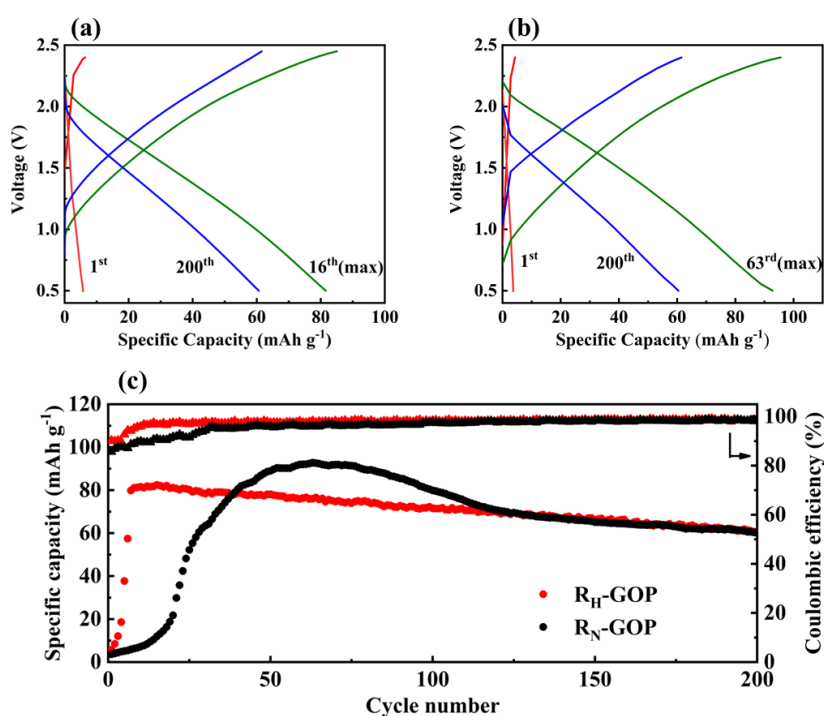


Figure 5. (a, b) Detailed charge and discharge curves of R_H-GOP and R_N-GOP cathode materials at different cycles (2 A g⁻¹). (c) Long-term stability tested for a R_H-GOP and R_N-GOP cathode materials at 2 A g⁻¹. All capacities of Al/R_H-GOP and Al/R_N-GOP batteries were recorded between charging and discharging voltages of 0.5 and 2.45 V.

Long-term stability tested for R_H-GOP and R_N-GOP cathode materials at were carried out at a current density of 2 A g⁻¹ (shown in Fig. 5c). It can be seen that the R_H-GOP exhibits a maximum discharge specific capacity after 15 activation cycles, while the activation of the R_N-GOP requires approximately 60 cycles. However, it is worth noting that the cycle life of the two materials is quite

different from those in previous reports [15]. After 200 cycles, the discharge specific capacities of the two materials decrease to approximately 60 mAh g⁻¹. It is well known that both the capacitance control process and the diffusion-control process exist in Al/graphene batteries [21]. The main chemical reaction of the diffusion-control process is due to the insertion of AlCl₄⁻ ions into the cathode material. Since the radius of the AlCl₄⁻ ion (5.8 Å) is much larger than that of the Li⁺ ion (0.76 Å), when the AlCl₄⁻ ion gradually increases to the intercalation/deintercalation of graphene, it will adversely affect the two graphene paper materials. The AlCl₄⁻ ions continue to enter the host materials as the charging voltage increases, which has been confirmed by Bhauriyal [10]. If the host materials eventually become a single layer of graphite intercalation compounds (GICs), the graphite layer expands by 163%, which will inevitably damage the cathode and ultimately accelerate the disintegration of the host material. Therefore, the two chemically reduced graphene papers failed to exhibit satisfactory cycle results. Correspondingly, since R_H-GOP and R_N-GOP have no obvious graphitization structure, the capacitance control process and the diffusion-control process in the battery needed to be quantitatively analyzed by CV curves.

Table 2. Comparison of electrochemical performances of certain selected cathode materials in Al-ion batteries.

| Cathode material | Discharge voltage (V) | Storage capacity (mAh g ⁻¹) | Current rate (mA g ⁻¹) | Cycle no. | Ref. |
|----------------------|-----------------------|---|------------------------------------|-----------|-----------|
| Graphene foam | ~ 1.8 | 60 | 4000 | 7500 | [5] |
| Graphene Nanoribbons | ~ 1.8 | 123 | 5000 | 10000 | [19] |
| Graphene film | ~ 2 | 100 | 5000 | 25000 | [20] |
| Graphene film | ~ 2 | 110 | 10000 | 250000 | [21] |
| Graphene film | ~ 2 | ~ 70 | 4800 | 10000 | [26] |
| Graphene film | - | ~ 90 | 2000 | 200 | This work |

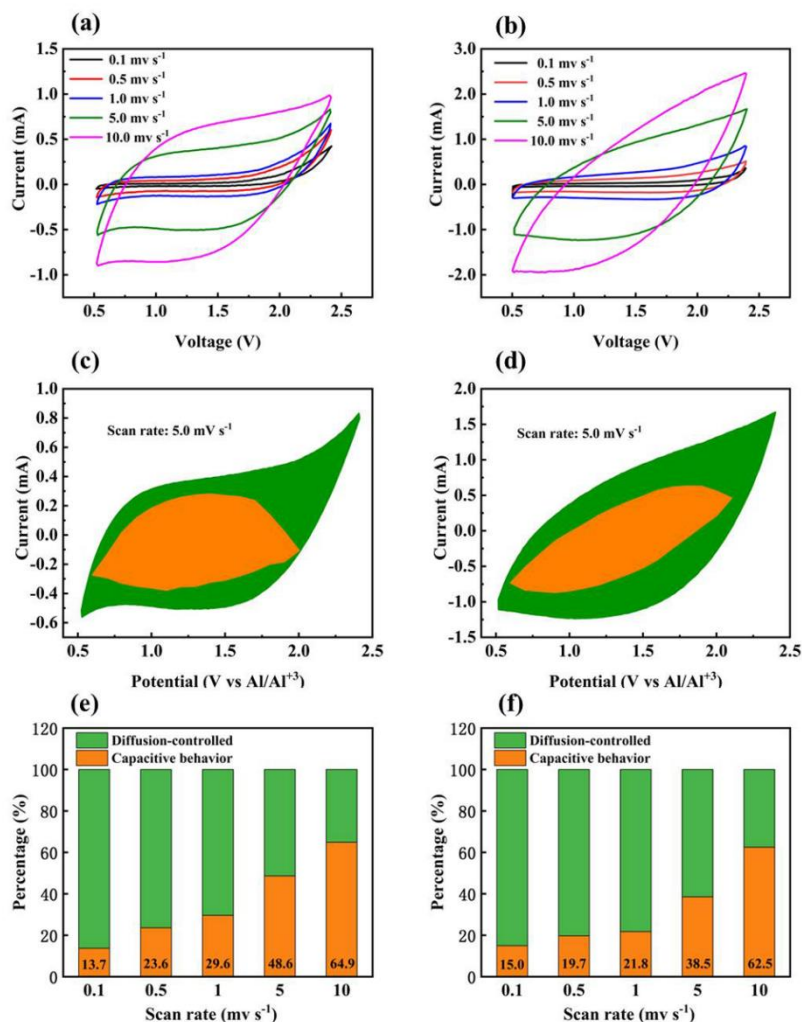


Figure 6. Cyclic Voltammetry of R_H-GOP and R_N-GOP cathode materials under different scan rate and 0.5-2.45 V vs. Al/Al³⁺: (a) Scan rates for R_H-GOP cathode are 0.1 (black), 0.5 (red), 1 (blue), 5 (green) and 10 (pink) mV s⁻¹. (b) Scan rates for R_N-GOP cathode are 0.1 (black), 0.5 (red), 1 (blue), 5 (green) and 10 (pink) mV s⁻¹. (c, d) Separation of the capacitive currents (expressed as orange) and diffusion-controlled currents (expressed as green) for R_H-GOP and R_N-GOP cathode materials at the scan rate of 5 mV s⁻¹. (e, f) The capacitive and diffusion contribution ratio of R_H-GOP and R_N-GOP cathode materials in the total intercalated charge as a function of sweep rates during CV processes.

It is worth mentioning that the previous reports must be charge-discharge tested at high current density, including this work (as shown in Table 2). To investigate the overall pseudo-capacitive behavior of R_H-GOP and R_N-GOP, a quantitative analysis of the charge storage generated by the capacitive process and the diffusion-control reaction is performed (as shown in Fig. 6). Fig. 6 (a, b) depicts the cyclic voltammetry (CV) curve of R_H-GOP (17th cycle) and R_N-GOP (74th cycle) in a pouch battery with a scan rate of 0.1-10.0 mV s⁻¹ between 0.5 and 2.4 V. The CV curve of R_H-GOP has a distinct anodic peak when the scan voltage is higher than 2.0 V, which indicates that HI reduces the graphene paper more thoroughly [32]. It is worth noting that the CV curves of the two materials have no obvious multiple anodic and cathodic peaks, which is different from the previous Al/graphene

batteries [7]. Therefore, it is necessary to clarify the charge reserves arising from the capacitance control process and diffusion-control process. Generally, the relationship between the measured peak current (i , in A) and the scan rate (v , in mV s^{-1}) is expressed by the following equation [33]:

$$i = av^b \quad (1)$$

When the electrochemical reaction is dominated by the diffusion-controlled process, the value of coefficient b is close to 0.5. Similarly, when the electrochemical reaction is dominated by the capacitive process, the value of coefficient b is 1 [33,34]. In fact, the Al/graphene battery had both a diffusion-controlled process and a capacitive process. The measured peak current (i_c) can be expressed as follows:

$$i_c = k_1v + k_2v^{\frac{1}{2}} \quad (2)$$

$$i_c / v^{\frac{1}{2}} = k_1v^{\frac{1}{2}} + k_2 \quad (3)$$

Based on the above two equations, i_c is determined by the capacitance process (k_1) and the diffusion-control process (k_2). Both k_1 and k_2 are constants, where the value of k_1 determines the contribution of the capacitive process. It can be seen from equation (3) that the relationship between $i_c/v^{1/2}$ and $v^{1/2}$ can be plotted during AlCl_4^- intercalation and deintercalation of the cathode material (R_H -GOP and R_N -GOP), wherein the slope (k_1) can be obtained by linear fitting. Then, the calculated k_1 value is applied to equation (1), and the charge storage amount is generated by the integral function calculation of the capacitance process. Correspondingly, at different scan rates, the ratio of the calculated curve area to the original CV curve area can reflect the capacitance process ratio.

As shown in Figs. 6 (c, d), the area of the selected curve (shown in orange) arises from the capacitance process of R_H -GOP and R_N -GOP at a scanning rate of 5.0 mV s^{-1} . At the same scan rate, the capacitance process of both materials is below 2.1 V. Furthermore, the amounts of charge storage produced by the capacitive process and the diffusion-control process at all scan rates for both materials are compared (Figs. 6e, f). As the scan rate increases from 0.1 to 10.0 mV s^{-1} , both materials exhibit a significant increase in charge storage arising from the capacitive process. Interestingly, the capacitance charge storage in both the Al/ R_H -GOP and Al/ R_N -GOP batteries exceeded 60% at a scan rate of 10.0 mV s^{-1} , which is a relatively high value. It is worth noting that the previous report considered that the Al/graphene battery is recognized as having pseudo-capacitive behavior [21], but only our study quantifies the capacitive process in the Al/graphene battery. Since the self-discharge phenomenon is a common feature of all pseudo-capacitive carbonaceous electrodes [35], the real reason Al/graphene batteries cannot be charged at low current densities may be due to the self-discharge of carbonaceous electrodes.

4. CONCLUSIONS

Self-supporting graphene paper (R_H -GOP and R_N -GOP) was prepared from graphene oxide by two common reduction methods (hydrogen iodide and hydrazine vapor) for Al/graphene battery research. In the 200 cycles, both cathode materials require an activation process in which the R_N -GOP cathode requires more cycles to fully release the full specific capacity. R_H -GOP and R_N -GOP cathodes enable the delivery of maximum specific capacities of 81.2 (16^{th} cycle) and 92.8 mAh g^{-1} (63^{rd} cycle), respectively, at a current density of 2 A g^{-1} . It is worth noting that the ratios of the capacitive

controlling process to the diffusion controlling process of the R_H-GOP and R_N-GOP cathode are 48.6% and 38.5%, respectively, at a scanning rate of 5.0 mV s⁻¹ by CV analysis. When the scanning rate is from 0.1 to 10.0 mV s⁻¹, this ratio increases with the scanning rate. The results confirm that the Al/graphene battery is primarily a pseudo-capacitive reaction and that it is both a capacitive process and a diffusion-control process. The capacitive process may be the reason why the Al/graphene battery must be charged/discharged at higher current densities.

ACKNOWLEDGEMENT

This work was supported by Jiangsu University [5501670001]; Natural Science Foundation of the Higher Education Institutions of Jiangsu Province [18KJB430010]; and the Dual Creative Doctoral Project of Jiangsu Province.

References

1. Q. Li, N.J. Bjerrum, *J. Power Sources*, 110 (2002) 1-10.
2. D. Liu, X. Fan, Z. Li, T. Liu, M. Sun, C. Qian, M. Ling, Y. Liu, C. Liang, *Nano Energy*, 58 (2019) 786-796.
3. P.R. Gifford, J.B. Palmisano, *J. Electrochem. Soc.*, 134 (1987) 610-614.
4. N. Jayaprakash, S.K. Das, L.A. Archer, *Chem. Commun.*, 47 (2011) 12610-12612.
5. M.C. Lin, M. Gong, B. Lu, Y. Wu, D.Y. Wang, M. Guan, M. Angell, C. Chen, J. Yang, B.J. Hwang, H. Dai, *Nature*, 520 (2015) 325-328.
6. Y. Gao, C. Zhu, Z. Chen, G. Lu, *J. Phys. Chem. C* 121 (2017) 7131-7138.
7. S.C. Jung, Y. Kang, D. Yoo, J.W. Choi, Y. Han, *J. Phys. Chem. C*, 120 (2016) 13384-13389.
8. H. Sun, W. Wang, Z. Yu, Y. Yuan, S. Wang, S. Jiao, *Chem. Commun. (Cambridge, U. K.)*, 51 (2015) 11892-11895.
9. S. Jiao, H. Lei, J. Tu, J. Zhu, J. Wang, X. Mao, *Carbon*, 109 (2016) 276-281.
10. P. Bhauriyal, A. Mahata, B. Pathak, *Phys. Chem. Chem. Phys.*, 19 (2017) 7980-7989.
11. H. Lei, J. Tu, Z. Yu, S. Jiao, *ACS Appl. Mater. Interfaces*, 9 (2017) 36702-36707.
12. D.Y. Wang, C.Y. Wei, M.C. Lin, C.J. Pan, H.L. Chou, H.A. Chen, M. Gong, Y. Wu, C. Yuan, M. Angell, Y.J. Hsieh, Y.H. Chen, C.Y. Wen, C.W. Chen, B.J. Hwang, C.C. Chen, H. Dai, *Nat. Commun.*, 8 (2017) 14283.
13. S. Wang, S. Jiao, W. Song, H. Chen, J. Tu, D. Tian, H. Jiao, C. Fu, D. Fang, *Energy Storage Materials*, 12 (2018) 119-127.
14. J. Wei, W. Chen, D. Chen, K. Yang, *J. Mater. Sci. Technol.*, 34 (2018) 983-989.
15. J. Qiao, H. Zhou, Z. Liu, H. Wen, J. Yang, *Ionics*, 25 (2019) 1235-1242.
16. M. Walter, K.V. Kravchyk, C. Bofer, R. Widmer, M.V. Kovalenko, *Adv. Mater.*, 30 (2018) e1705644.
17. Y. Wu, M. Gong, M.C. Lin, C. Yuan, M. Angell, L. Huang, D.Y. Wang, X. Zhang, J. Yang, B.J. Hwang, H. Dai, *Adv. Mater.*, 28 (2016) 9218-9222.
18. G.Y. Yang, L. Chen, P. Jiang, Z.Y. Guo, W. Wang, Z.P. Liu, *RSC Adv.*, 6 (2016) 47655-47660.
19. X. Yu, B. Wang, D. Gong, Z. Xu, B. Lu, *Adv. Mater.*, 29 (2017) 1604118.
20. H. Chen, F. Guo, Y. Liu, T. Huang, B. Zheng, N. Ananth, Z. Xu, W. Gao, C. Gao, *Adv. Mater.*, 29 (2017) 1605958.
21. H. Chen, H. Xu, S. Wang, T. Huang, J. Xi, S. Cai, F. Guo, Z. Xu, W. Gao, C. Gao, *Sci. Adv.*, 3 (2017) eaao7233.
22. X. Huang, Y. Liu, H. Zhang, J. Zhang, O. Noonan, C. Yu, *J. Mater. Chem. A*, 5 (2017) 19416-19421.
23. P. Wang, H. Chen, N. Li, X. Zhang, S. Jiao, W. Song, D. Fang, *Energy Storage Materials*, 13 (2018) 103-111.

24. Z.A. Zafar, S. Imtiaz, R. Li, J. Zhang, R. Razaq, Y. Xin, Q. Li, Z. Zhang, Y. Huang, *Solid State Ionics*, 320 (2018) 70-75.
25. H. Li, H. Yang, Z. Sun, Y. Shi, H.M. Cheng, F. Li, *Nano Energy*, 56 (2019) 100-108.
26. L. Zhang, L. Chen, H. Luo, X. Zhou, Z. Liu, *Adv. Energy Mater.*, 7 (2017) 1700034.
27. D.A. Dikin, S. Stankovich, E.J. Zimney, R.D. Piner, G.H. Dommett, G. Evmenenko, S.T. Nguyen, R.S. Ruoff, *Nature*, 448 (2007) 457-460.
28. D. Luo, G. Zhang, J. Liu, X. Sun, *J. Phys. Chem. C*, 115 (2011) 11327-11335.
29. S. Pei, J. Zhao, J. Du, W. Ren, H.M. Cheng, *Carbon*, 48 (2010) 4466-4474.
30. I.K. Moon, J. Lee, R.S. Ruoff, H. Lee, *Nat. Commun.*, 1 (2010) 73.
31. C.N.R. Rao, A.K. Sood, K.S. Subrahmanyam, A. Govindaraj, *Angew. Chem., Int. Ed.*, 48 (2010) 7752-7777.
32. S. Pei, H.M. Cheng, *Carbon*, 50 (2012) 3210-3228.
33. M. Lübke, A. Sumboja, I.D. Johnson, J.L.B. Dan, P.R. Shearing, Z. Liu, J.A. Darr, *Electrochim. Acta*, 192 (2016) 363-369.
34. V. Augustyn, J. Come, M.A. Lowe, J.W. Kim, P.L. Taberna, S.H. Tolbert, H.D. Abruña, P. Simon, B. Dunn, *Nat. Mater.*, 12 (2013) 518.
35. X. Fan, Y. Li, S. Wang, Y. Lu, H. Xu, J. Liu, C. Yan, *Electrochim. Acta*, 176 (2015) 70-76.

© 2019 The Authors. Published by ESG (www.electrochemsci.org). This article is an open access article distributed under the terms and conditions of the Creative Commons Attribution license (<http://creativecommons.org/licenses/by/4.0/>).